ARL-TR-8144 ● Sep 2017

US Army Research Laboratory

Synthesis of Bilayer Graphene on 90/10 Copper (Cu)/Nickel (Ni) Alloy and Transfer by Electrochemical Delamination

by Eugene Zakar, Robert Burke, and Madan Dubey

NOTICES

Disclaimers

The findings in this report are not to be construed as an official Department of the Army position unless so designated by other authorized documents.

Citation of manufacturer's or trade names does not constitute an official endorsement or approval of the use thereof.

Destroy this report when it is no longer needed. Do not return it to the originator.

ARL-TR-8144 ● Sep 2017

US Army Research Laboratory

Synthesis of Bilayer Graphene on 90/10 Copper (Cu)/Nickel (Ni) Alloy and Transfer by Electrochemical Delamination

by Eugene Zakar and Madan Dubey
Sensors and Electron Devices Directorate, ARL

Robert Burke
General Technical Services, LLC, Wall, NJ

REPORT DOCUMENTATION PAGE

Form Approved
OMB No. 0704-0188

1. REPORT DATE *(DD-MM-YYYY)*	2. REPORT TYPE	3. DATES COVERED (From - To)
September 2017	Technical Report	1 September 2016–31 August 2017

4. TITLE AND SUBTITLE
Synthesis of Bilayer Graphene on 90/10 Copper (Cu)/Nickel (Ni) Alloy and Transfer by Electrochemical Delamination

5a. CONTRACT NUMBER

5b. GRANT NUMBER

5c. PROGRAM ELEMENT NUMBER

6. AUTHOR(S)
Eugene Zakar, Robert Burke, and Madan Dubey

5d. PROJECT NUMBER

5e. TASK NUMBER

5f. WORK UNIT NUMBER

7. PERFORMING ORGANIZATION NAME(S) AND ADDRESS(ES)
US Army Research Laboratory
ATTN: RDRL-SER L
2800 Powder Mill Road
Adelphi, MD 20783-1138

8. PERFORMING ORGANIZATION REPORT NUMBER
ARL-TR-8144

9. SPONSORING/MONITORING AGENCY NAME(S) AND ADDRESS(ES)

10. SPONSOR/MONITOR'S ACRONYM(S)

11. SPONSOR/MONITOR'S REPORT NUMBER(S)

12. DISTRIBUTION/AVAILABILITY STATEMENT
Approved for public release; distribution is unlimited.

13. SUPPLEMENTARY NOTES

14. ABSTRACT
This study reports the growth of bilayer graphene on 90/10 copper/nickel alloy foils and thin films by chemical vapor deposition. We also describe an electrochemical delamination method that does not rely on etching of the underlying metal for release of the graphene layer. Instead, hydrogen bubble evolution is used to separate the graphene at the metal/graphene interface. The bubble delamination process overcomes difficulties associated with traditional wet etching of the metal, allowing major reductions in processing time and generation of hazardous chemical waste. Furthermore, since the metal catalyst is not consumed in the process, it can be recycled. The graphene can be transferred to a rigid or flexible substrate. We evaluate the quality of graphene transferred from a metal foil and metal film to a host silicon dioxide/silicon substrate by micro Raman and optical microscopy imaging methods.

15. SUBJECT TERMS
graphene, chemical vapor deposition, CVD, growth, transfer, electrochemical, delamination

16. SECURITY CLASSIFICATION OF:			17. LIMITATION OF ABSTRACT	18. NUMBER OF PAGES	19a. NAME OF RESPONSIBLE PERSON
a. REPORT	b. ABSTRACT	c. THIS PAGE			Eugene Zakar
Unclassified	Unclassified	Unclassified	UU	24	19b. TELEPHONE NUMBER (Include area code) (301) 394-1628

Standard Form 298 (Rev. 8/98)
Prescribed by ANSI Std. Z39.18

Contents

List of Figures

List of Tables

1. Introduction

Chemical vapor deposition (CVD) is one of the most promising methods for growth of large-area graphene on catalyst surfaces such as copper (Cu) and nickel (Ni) as these metals are cheap, compatible, and adaptable to existing semiconductor technologies.[1,2]

Graphene could be used in a lot of different applications, but it needs to be transferred from the metal surface, where it was grown, to silicon dioxide (SO_2)[3,4] or a flexible polymer host substrate for it to be useful. The properties of graphene can further be enhanced by the fact that carbon (C) is a backbone that can be covalently or noncovalently functionalized with heteroatoms (noncarbon atoms), as it unlocks the potential of tailoring its electrochemical and electrical properties to cater to various applications.

However, for electronic field-effect transistor (FET) applications,[3,5,6] a sheet or single layer of graphene does not have a bandgap, which limits its usefulness. The formation of a bandgap is required so that the electrical current in a circuit can be shut off in the off-state. A bandgap can be generated by an electric bias applied perpendicular to bilayer graphene (BLG) without structural confinement.[7] Additionally, when more than one layer of graphene is used as a contact material in FET applications, improvements are found in the contact resistance and sheet resistance of the electronic devices.[8,9] The covalent/ionic bonds formed between metal and carbon atoms allow for a lower contact resistivity compared to the weak van de Waals bonds under conventional top contacts.[10]

Graphene growth on pure Cu foil is known to be single layer due to its low C solubility (0.001% at 1,000 °C) and slow decomposition rate in methane (CH_4).[11] Cu alone has sometimes been shown to form incomplete bilayers with a significant fraction of non-AB stacking.[12–17]

CuNi alloys in the form of foils[18,19] and thin films[20–22] have been used for growth of BLG. The addition of Ni to the Cu improves BLG coverage due to the higher C solubility (~1.3% at 1,000 °C) in the Ni constituent when using a CH_4 gas source.[23] Direct comparisons of graphene growth from the 2 forms of metal, foil and thin film of the same composition, under the same growth conditions of pressure, temperature, and gas flows, are not readily available, which is one of the main objectives of this study. We selected commercial 90/10 Cu/Ni foil and compared it to in-house-prepared thin films of the same composition.

2. Methods

2.1 Growth of Graphene

A metal foil composed of 90% Cu and 10% Ni (CA 706, 5-mil thickness) was purchased from Midwest Metals Inc. Metal films (600-nm thickness) of the same composition were prepared in-house by sputter coating Cu and Ni on a thermally oxidized silicon (Si) substrate (280-nm SiO_2) using an AJA International model ATC-2200 system. The process of co-depositing Cu and Ni thin films, alloying, composition analysis, surface roughness measurements, and texture evaluations have been detailed in a previous report.[24]

The commercial foils were cleaned by soaking them in acetone for 30 min, followed by isopropyl alcohol. The metal thin films deposited on SiO_2/Si substrates were not cleaned prior to graphene growth. After cleaning, the samples were loaded directly into the center of a quartz tube furnace for growth. The system was pumped down and then brought to a pressure of 600 Torr using a gas mixture of 65 sccm hydrogen (H_2) and 150 sccm argon (Ar). The furnace was heated to 500 °C, and the samples were annealed for 30 min before heating to 1,075 °C and holding there for 10 min to increase the metal grain size. Afterwards, first-layer graphene growth by surface absorption method was carried out at 1,075 °C for 10 min with the addition of 0.5 vol% CH_4. Then, the second-layer graphene growth by segregation method was carried out by cooling at a rate of 5 °C/min to 900 °C and held there for 60 min. After completion of the 2-layer graphene growth, the chamber temperature was cooled at a rate of 5 °C/min until 500 °C and then readjusted to 50 °C/min until reaching room temperature. The gases were turned off at room temperature and the substrates removed.

2.2 PMMA Coating

Several techniques are used to release and transfer the graphene from the metal catalyst, among them a polymer supportive layer-based poly(methyl methacrylate) (PMMA). The PMMA-supported method is the most widely used transfer process at present for graphene prepared by CVD. The thickness of the PMMA layer can be adjusted by changing the spinning rate and the concentration of PMMA solution. In addition, PMMA is also suitable for a supporting layer that can be easily removed by either acetone and/or annealing without damaging the underlying graphene. The PMMA consequently leaves residues on the graphene surface after the removal process. The PMMA concentration in anisole solution is an important evaluation

criterion. We evaluated MicroChem brand molecular weight 950K PMMA diluted in 9%, 8%, and 4% anisole solution, respectively.

2.3 Transfer Methods

Separation of graphene from the metal foil substrate involves chemical etching of the underlying metal. The chemical etching process typically requires several hours to remove the metal depending on its thickness, which increases the production cost and causes environmental concerns. We describe a conventional wet etch process and an improved electrolytic bubble transfer method in the following sections.

2.3.1 Conventional Etch

With metal foils, where CVD graphene is grown on both sides, only the top side of the foil is coated with PMMA. The graphene on backside of the metal foil is removed by exposing it to an oxygen (O_2) plasma for 2 min. After baking this PMMA/graphene/Cu foil stack in an air oven at 80 °C for 15 min, it was brought to an iron chloride ($FeCl_3$)-based aqueous Cu etchant (CE-100, TRANSENE) bath until the Cu foil was completely etched. The resulting PMMA/graphene stack was carefully rinsed with deionized (DI) water and subsequently soaked into 10% hydrogen chloride (HCl) solution for 10 min to remove metallic salts from the previous etch and finally rinsed with DI water again. The PMMA/graphene is then transfer to an arbitrary SiO_2/Si or flexible substrate and dried overnight. The PMMA is removed by a 30-min acetone soaking step, followed by a 3-h thermal anneal at 350 °C informing gas (4% H_2/96% Ar) flowing at 1500 sccm.

When using metal films deposited on a SiO_2/Si substrate, the same procedure is followed but without the O_2 plasma step, since only one side of the metal has been exposed to graphene growth.

2.3.2 Electrochemical

With metal foils where CVD graphene is grown on both sides, PMMA must be coated on both sides so that the forces from the electrochemical H_2 bubbling formation are of equal strength on both sides. Strong alkalis and acids, such as sodium hydroxide, potassium hydroxide (KOH), and sulfuric hydroxide are good candidates that create H_2 bubbles in water electrolysis reactions. However, considering that Cu and CuNi metals can strongly react with chemicals, we used a diluted 1-M KOH electrolyte solution[25] to limit the reaction of the metal foil with the solution. The CuNi foils react minimally when exposed to diluted KOH, but H_2 bubbling is visible on both electrodes when immersed in the electrolyte solution with an applied electrical potential between –3 to –5 V.

2.4 Characterization

After transfer, the morphology of the graphene surface was evaluated by an atomic force microscope (AFM) (Veeco NanoScope V) in the tapping mode. Raman spectroscopy using a WITec Alpha 300RA system was carried out to look at the graphene quality and layer count. The Raman spectra were measured in the backscattering configuration using the 532-nm line of a frequency-doubled neodymium:yttrium aluminum garnet laser as the excitation source (~1.5 mW at sample), with a 100× objective and 600 grooves/mm grating with a 0.5-s integration time.

3. Results

3.1 PMMA Coating

A PMMA scaffold must have good adhesion to the graphene film and be resilient to mechanical handling during the transfer process. We evaluated PMMA with different concentrations in anisole solution. The selection of an optimum PMMA concentration was based on determining which PMMA led to the least amount of residues left behind on the graphene surface after the PMMA removal step by acetone soaking. According to previous experiments conducted by other research groups,[26] the minimum acceptable layer thickness for PMMA is 600 nm; therefore, we decided to target a thickness of 1 μm to be safe. A tradeoff exists between the thickness and the flexibility of the PMMA layer. If the PMMA layer is thinner than 600 nm, the transfer created pores and tears in the graphene layer. A much thicker layer, on the other hand, produced nonconformities in the transferred graphene. Since the PMMA viscosity varies based on concentration in anisole, appropriate spin coating speeds were developed for each PMMA product to reach a desired thickness of 1 μm (Table 1). PMMA A9 with relatively high spin speed achieved a final thickness of 1.5 μm, while PMMA A4 with relatively low spin speed needed 3 coatings to achieve a 1.1-μm layer.

Table 1 950K PMMA thickness and characteristics

PMMA type	Target thickness (μm)	Spin speed ×1000 (RPM)	Final thickness (μm)	Surface roughness (nm)
A9	1	3.5	1.5	4.59
A8	1	2.5	1.2	4.01
A4	1	1.0 (3 times)	1.1	2.07

Among the various PMMAs tested, we selected PMMA-A4 as it produced the least amount of residues after soaking in acetone for 30 min, according to AFM images shown in Fig. 1. Increasing the soaking times and annealing the graphene samples in forming gas greatly diminishes the final amount of visible residues on the surface of graphene.

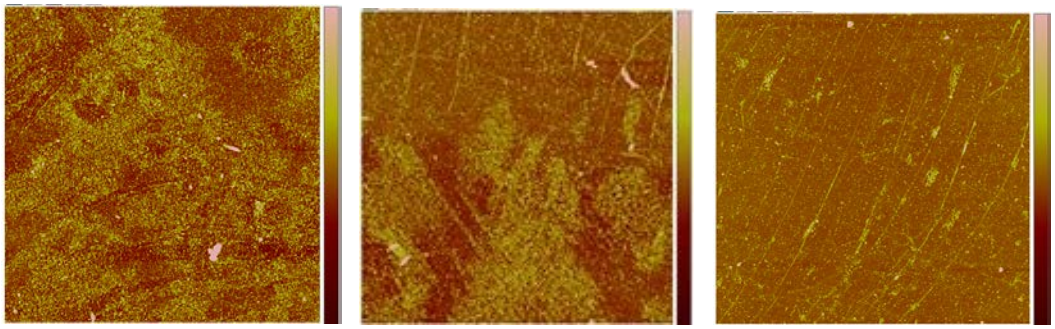

(a) (b) (c)

Fig. 1 AFM image of residues (white) on the surface of graphene after removal of a) 9% PMMA in anisole, b) 8% PMMA in anisole, and c) 4% PMMA in anisole. The image size is 10 µm on the side and the adjacent height scale bar is 40 nm.

3.2 Transfer of Graphene

After the growth of graphene on a metal foil and metal film, different methods were employed for separation of the graphene from the metal. We compared conventional chemical etching to electrolytic delamination methods[27–29] for the transfer of graphene to an arbitrary substrate.

3.2.1 Conventional Etch

Conventional chemical etching of Cu based foils can be time consuming as it requires several steps including O_2 plasma for removing graphene from one side of the foil, followed by $FeCl_3$ to etch to consume the entire metal. Nano iron (Fe) impurities that are strongly adsorbed onto the graphene and cannot be completely removed will have a strong influence on the electronic and electrochemical properties of graphene.[30–32] Additional soaking in 10% HCl solution removes the Fe residues. This conventional wet etching method becomes unreliable when the starting metal foil is greater than 1 mil in thickness, since it requires etching the sample overnight. If a metal alloy is used, a reliable chemistry must to be selected that etches both constituents of the metal equally well.

Alternatively, separation of graphene from a metal film (~1 µm) on an SiO_2/Si substrate is challenging. Undercut etching is a very slow and tedious process because the metal film is sandwiched between the top PMMA coating and the

substrate, leaving only a fraction of the metal edges exposed to the chemical etch and can easily take over 24 h to remove. The etching is further hampered by defects, impurities and contamination in the metal film.

3.2.2 Electrochemical

Recently authors Wang,[33] Gao,[34] and de la Rosa[35] have suggested a transfer technique based on the separation of graphene from metal foils by H_2 bubble formation. An advantage of the bubble transfer process is that it eliminates 3 etching steps from the conventional wet etch: the backside foil O_2 plasma etch, the $FeCl_3$ metal wet etch, and HCl etch steps. The electrolytic delamination process reduces the cost and handling of chemical hazardous waste as it is completely independent of the metal thickness and enables use of noble metals such as platinum that cannot be easily etched. We used an electrolytic cell consisting of a KOH electrolyte with a PMMA/graphene/metal stack as the cathode. An illustration of the electrolytic delamination process is shown in Fig. 2a with an image of the actual setup in Fig. 2b. The setup consists of a direct current power supply (left), an electrochemical cell (center), and a clamping sample holder mounted to a multidirectional mechanical manipulator on the cathode side (right).

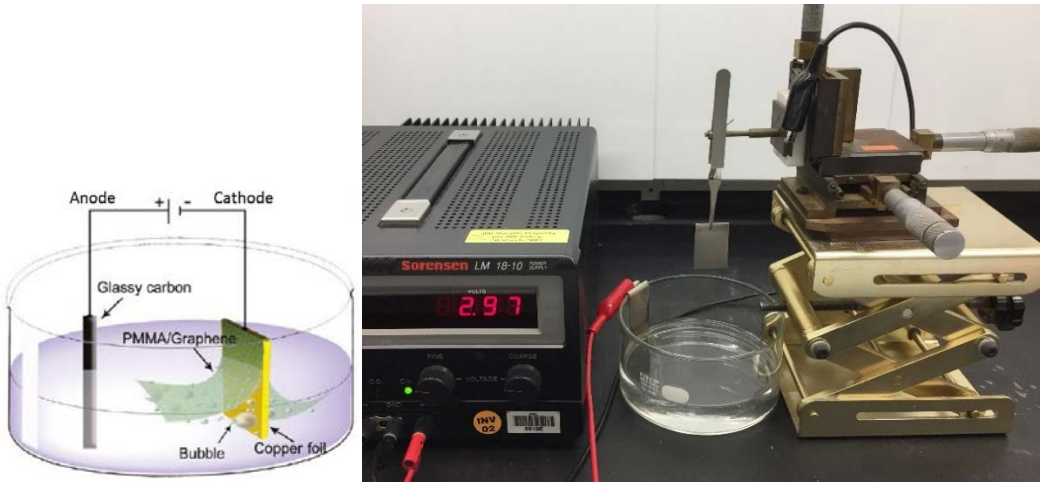

(a) (b)

Fig. 2 Electrochemical transfer of graphene in a) illustration and b) actual setup in the laboratory

The PMMA/graphene/metal stack was slowly lowered into an aqueous KOH electrolyte solution with help of the cathode clamp holder with an applied electrical potential of –3 V, causing the reduction of water and producing H_2 bubbles ($2H_2O + 2e^- \rightarrow H_2 + 2OH^-$). The H_2 bubbles generated at the graphene/metal interface serve to delaminate the graphene film from the metal foil, starting from the bottom edges exposed to the electrolyte and progressing up to the rest of the

film due to electrolyte permeation into the interlayers. Increasing the electrical potential to the cathode resulted in faster delamination.

However, with electrochemical H_2 bubbling, mechanical damage to the graphene film can occur due to the surface tension of bubbles at the PMMA/graphene interface.[35,36] Therefore, the bubbling rate must be controlled; otherwise, defects such as holes and cracks (as shown in Fig. 3) can occur in the graphene layer due to the bubble transfer process.

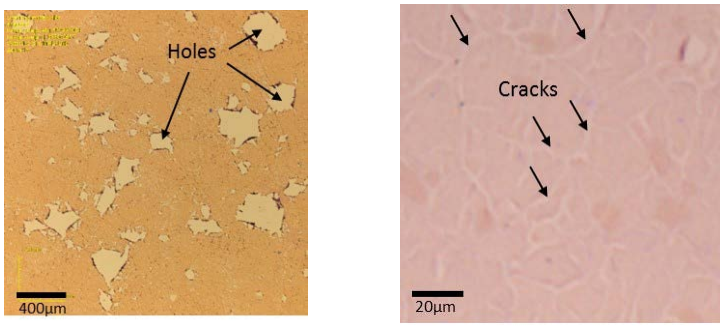

(a) (b)

Fig. 3 Image of defects in graphene after the transfer process: a) holes and b) cracks

To avoid the formation of H_2 bubbles altogether and greatly reduce damage to the graphene during the transfer process, Cherian et al. developed a bubble-free electrochemical delamination method.[37] This bubble-free method exploits the selective etching of cuprous oxide (Cu_2O) formation on a Cu foil surface ($Cu_2O + H_2O + 2e^- \rightarrow 2Cu + 2OH^-$) by holding the PMMA/graphene/Cu stack at a lower electrical potential than previously applied. In the absence of mechanical forces originally provided by the bubbles, a gradual immersion technique was used, where the initially delaminated PMMA/graphene stack floating on the solution provided the driving force instead. We adapted this approach to our electrolytic delamination and found the potential needed to eliminate bubbling altogether occurs between –0.5 to –1.5 V according to our current-voltage (I-V) calibration plot (Fig. 4) for a 1-M KOH electrolyte solution. These values can shift depending on the electrolyte concentration, electrode material, and sample size.

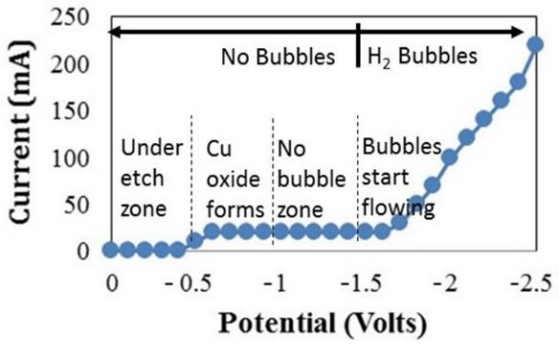

Fig. 4 Calibration curve showing the zones for H_2 bubble evolution in 1-M KOH electrolyte solution

We see from the I-V calibration plot that increasing the electrical potential beyond approximately –1.5 V started the evolution of microbubbles on electrode surfaces followed by a vigorous flow of H_2 bubbles at much higher potentials. Bubble-free delamination occurred at approximately –1.25 V and slowed down the process to approximately 1 h, but it is still a 24 times improvement in time over the conventional metal wet etch method, which can take over 24 h for thick metals. The amount of defects in the graphene film is also reduced by the bubble-free method. When the potential fell below approximately –1 V, the cathode was brown in color and appeared heavily oxidized, and the delamination time began to degrade rapidly. Figure 5 shows images during the process of graphene delamination as function of cathode potential.

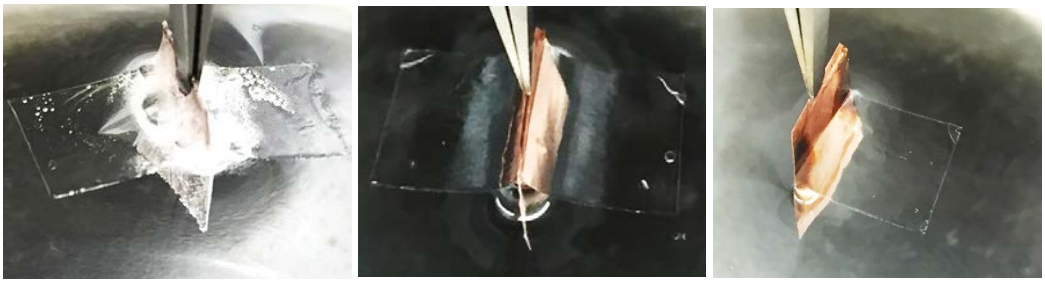

(a) (b) (c)

Fig. 5 Image of a PMMA/graphene stack in the process of electrochemical delamination from a metal foil at cathode potential a) –3 V, b) –1.25 V, and c) –1 V

3.3 Raman Spectroscopy Analysis of Graphene

Micro-Raman spectroscopy is already established as a powerful tool to characterize defects and the number of graphene layers. In Raman spectra of graphene, the main features are the G-band mode (~1590 cm^{-1}), the G'-band mode (~2690 cm^{-1}), and the D-band mode or the disorder-induced band (1350 cm^{-1}). By observing the differences in the G'- and G-band intensity ratios, and the G'-band wavenumber

(peak width) and line shape, the number of graphene layers contained in graphene films can be obtained and also the stacking order or interlayer interactions in few-layer graphene films.[38] Graphene films grown from both thin films and foils were evaluated after transfer to SiO_2/Si substrates.

For single-layer graphene (SLG), the G' full width at half maximum (FWHM) is in the narrow range of 26–38 cm^{-1} and $I_{G'}/I_G$ ratio in the range of approximately 2.5–4.5, while for BLG, the distribution of the FWHM is in the wide range of 39–65 cm^{-1} (cut-off 70 cm^{-1}) and $I_{G'}/I_G$ ratio in the range of 0.5–2.2.

Figure 6a shows an optical image and Fig. 6b a Raman scanned image with $I_{G'}/I_G$ ratios for CVD growth of graphene on a thin-film metal sample 90Cu/10Ni alloy composition. The white scale bar on the bottom left represents 4 µm. The Raman scan shows an $I_{G'}/I_G$ ratio in the range 0.68 to 3.1, which represents both SLG and BLG. Furthermore, if we take 2 spot checks from the Raman scan, the first group of spectra with the green cross shown in Fig. 6c has a single-Lorentzian profile for the G' band, a narrow linewidth of 32 cm^{-1} at 2729 cm^{-1}, and an $I_{G'}/I_G$ greater than 2 that is characteristic of SLG. On the other hand, the second group of spectra with the red cross has a broader G' band (~58 cm^{-1}), and an $I_{G'}/I_G$ of approximately 1 that is well representative of BLG. Both groups of spectra demonstrate the distinguishing characteristic features of SLG and BLG as expected. The nonexistent intensity of the D band (~1350 cm^{-1}) on both the spectrum confirms the graphene has low defects. The amount of BLG coverage (range of 39–65 cm^{-1}) is roughly a third compared to SLG (range of 26–38 cm^{-1}) according to the FWHM distribution curve in Fig. 6d.

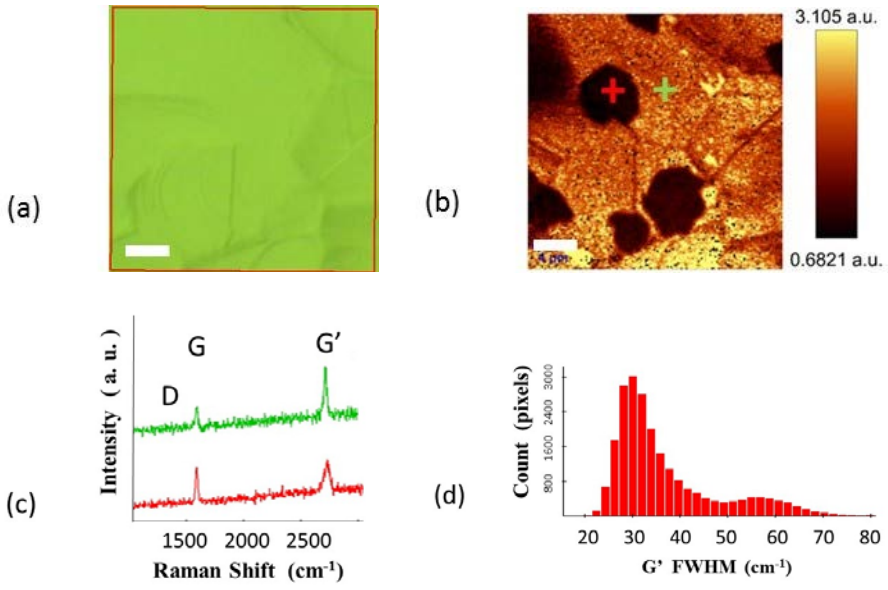

Fig. 6 Analysis of graphene growth from a metal film a) optical image, b) $I_{G'}/I_G$ ratio scan, c) Raman spectra, and d) G' FWHM distribution. The white scale bar represents 4 µm.

Figure 7a shows an optical image and Fig. 7b a Raman scanned image of graphene grown on metal foils with same 90Cu/10Ni alloy composition. The white scale bar on the bottom left represents 4 µm. The Raman scan shows an $I_{G'}/I_G$ ratio in the range 0.18 to 2.69, which is characteristic of SLG, BLG, and additional trilayer graphene (TLG). The Raman spectrum for the first group with the green cross shown in Fig. 7c has a G' band with narrow linewidth of 32 cm^{-1} and $I_{G'}/I_G$ greater than 2 that is representative of SLG. On the other hand, the second group of spectra with the red cross has $I_{G'}/I_G$ of approximately 1, as well as broadening of G' band line width (~58 cm^{-1}) that is representative of BLG. A third group of spectra with the blue cross has $I_{G'}/I_G$~0.32 as well as further broadening of G' band line width (~73 cm^{-1}) that are representative of TLG. The nonexistent intensity of the D band (~1350 cm^{-1}) confirms the graphene has low defects. The amount of BLG coverage (range of 39–65 cm^{-1}) is roughly a third compared to SLG (range of 26–38 cm^{-1}) according to the FWHM distribution curve in Fig. 7d.

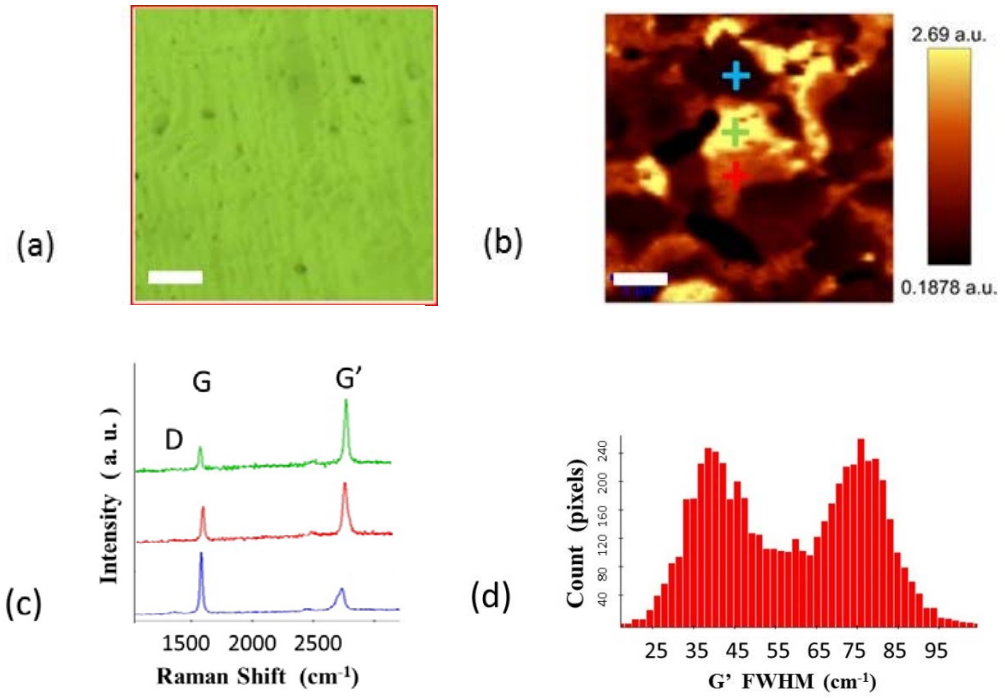

Fig. 7 Analysis of graphene growth from a metal foil a) optical image, b) $I_{G'}/I_G$ ratio scan, c) Raman spectra, and d) G' FWHM distribution. The white scale bar represents 4 µm.

3.4 Optical Inspection of Graphene

Small-area microanalysis is not always representative of the large-area sample. The differences in formation and distribution of graphene growth may be attributed due to differences in the metal grain boundaries, surface roughness, crystallography,

impurities, and so on. A large-area optical image 125 µm × 125 µm was taken from the same sample region as the Raman scan 20 µm × 20 µm from Fig. 6b. The larger-area optical image in Fig. 8a shows basically the same features of BLG spots and distribution across the entire surface. Therefore, the small-area Raman scan area in this case is representative of the entire surface graphene growth on the thin-film metal.

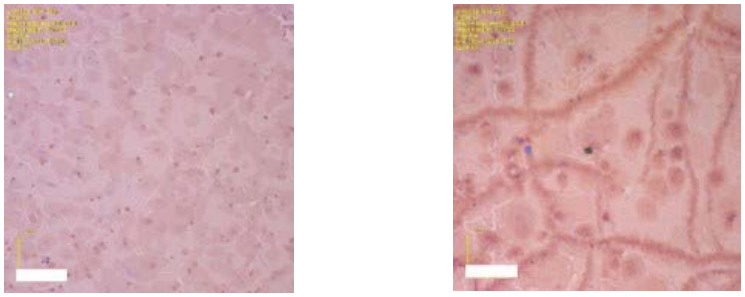

(a) **(b)**

Fig. 8 Optical image of graphene transferred to a host SiO_2/Si substrate from a) metal film and b) metal foil. The scale bar represents 20 µm.

For graphene growth on a foil metal sample, the small-area Raman scan from Fig. 7b does not fully represent the broad area optical image from Fig. 8b. The BLG growth on the large-area surface is not equally distributed as on the Raman scan. Additionally, dark vein-like structures appearing on the broad-area image are absent from the smaller Raman scan. The veins have a similar appearance to deep grains found in the original metal surface of the foil. The dark veins are identified as TLG according to Raman data from Fig. 7b. However, the veins are only captured on the larger-scale optical image due to their excessive separations beyond the scale of the Raman scan.

The absence of vein-like graphene structures from growth on thin films is partially due to the starting metal having smooth and shallow grain boundaries that allow uniform segregation of C to the surface shown in Fig. 8a. The thin-film metal has a low average surface roughness of 26 nm and a preferred (111) crystalline-oriented texture. In contrast, the starting foil has a high average roughness of 157 nm, and a mixed (200) and (220) orientated texture that allows the accumulation of C to form multilayer graphene on those sites by segregation. Formation of TLG vein-like features in Fig. 8b can be minimized to a great degree if the rough surfaces and deep grain boundaries found in commercial cold-rolled foils can be smoothened prior to the growth of the graphene. Electrochemical treatment of deep-grained Cu foil has been shown to improve the surface roughness,[39] more so than traditional mechanical polishing methods, and can be adapted to CuNi alloy foils provided the constituents can be etched uniformly.

4. Conclusions

The CVD growth of BLG on both foils and thin films with 90Cu–10Ni alloy composition has been demonstrated. However, with the foils, TLG begins to appear on the surface. The TLG growth is attributed to high surface roughness and deep grain boundaries found native to the starting material, which act as nucleation sites where C tends to segregate in greater concentrations. In this case, we recommend electro polishing of commercial foils to improve the smoothness level to several nanometers prior to the CVD growth of graphene.

An electrochemical process is described here that can overcome difficulties associated with wet etch release of CVD grown graphene from very thick and very thin-film metal catalyst surfaces. Several advantages are gained by use of electrochemical process over conventional etching release, including the following:

- No dependency on metal thickness (greatly reduces release time).
- Eliminates 3 chemical process steps (less chemical waste).
- Enables new capability for growth and release of graphene on noble metals like platinum that are inert to chemical etching.

5. References

1. Li X, Cai W, An J, Kim S, Nah J, Yang D, Piner R, Velamakanni A, Jung I, Tutuc E, Banerjee SK, Colombo L, Ruoff RS. Science. 2009;324:1312.
2. Liu W, Li H, Xu C, Khatami Y, Banerjee K. Carbon. 2011;49:4122.
3. Vlassiouk I, Regmi M, Fulvio P, Dai S, Datskos P, Eres G, Smirnov S. ACS Nano. 2011;5:6069.
4. Zahn Z, Sun J, Liu L, Wang E, Cao Y, Lindvall N, Skoblin G, Yurgens AJ Mater Chem C. 2015;3:8634–8641.
5. Bhaviripudi S, Jia X, Dresselhaus MS, Kong J. Nano Lett. 2010;10:4128.
6. Kim KS, Zhao Y, Jang H, Lee SY, Kim JM, Kim KS, Ahn JH, Kim P, Choi JY, Hong BH. Nature. 2009;457:706.
7. McCann E. Phys Rev B. 2006;74:161403.
8. Kwak BW et al. Physica E. 2015;68:33–37.
9. Leong et al. ACS Nano. 2015;9(1):869–877.
10. Matsuda Y, Deng W, Goddard WA. J Phys Chem C. 2010;114:17845–17850.
11. Lopez GA, Mittemeijer E. J Scr Mater. 2004;51:1.
12. Liu N, Fu L, Dai B, Yan K, Liu X, Zhao R, Zhang Y, Liu, Z. Nano Lett. 2011;11:297.
13. Reina A, Jia X, Ho J, Nezich D, Son H, Bulovic V, Dresselhaus MS, Kong J. Nano Lett. 2009;9:30.
14. Chen S, Cai W, Piner RD, Suk JW, Wu Y, Ren Y, Kang J, Ruoff RS. Nano Lett. 2011, 11, 3519.
15. Liu X, Fu L, Liu N, Gao T, Zhang Y, Liao L, Liu Z. J Phys Chem C. 2011;115:11976.
16. Wu Y, Chou H, Ji H, Wu Q, Chen S, Jiang W, Hao Y, Kang J, Ren Y, Piner RD, Ruoff RS. ACS Nano. 2012;6:7731.
17. Fang W, Hsu AL, Caudillo R, Song Y, Birdwell AG, Zakar E, Kalbac, Dubey M, Palacios MT, Dresselhaus MS, Araujo PT, Kong J. Nano Lett. 2013;13:1541.

18. Wu Y, Chou H, Ji H, Wu Q, Chen S, Jiang W, Hao Y, Kang J, Ren Y, Piner RD, Ruoff RS. ACS Nano. 2012. DOI 10.1021/nn301689m.

19. Chen S, Cai W, Piner RD, Suk JW, Wu Y, Ren Y, Kang J, Ruoff RS. Nano Lett. 2011;11:3519–3525.

20. Liu X. J Phys Chem C. 2011;115:11976–11982.

21. Liu Wei et al. Chem Mater. 2014;26 (2):907–915.

22. Takesaki Y et al. Chem Mater. 2016;28:4583−4592.

23. Cai W, R. Piner D, Zhu Y, Li X, Tan Z, Floresca HC, Yang C, Lu L, Kim JJ, Ruoff RS. Nano Res. 2009;2:851.

24. Zakar E, Chen A, Burke R, Hirsch SG, Strnad N, Mulcahy J.. Characterization of magnetron sputtered copper-nickel thin films and alloys. Adelphi (MD): Army Research Laboratory (US); 2016 Sept. Report No.: ARL-TR-7783.

25. Fisichella G, Di Franco S, Roccaforte F, Ravesi S, Giannazzo F. Appl Phys Lett. 2014;104:233105.

26. Zahn Z, Sun J, Liu L, Wang E, Cao Y, Lindvall N, Skoblin NG, Yurgens A. J Mater Chem. C. 2015;3: 8634-8641.

27. Yu QK, Jauregui LA, Wu W, Colby R, Tian JF, Su ZH, Cao HL et al. Nat Mater. 2011;10:443.

28. Reina A, Jia XT, Ho J, Nezich D, Son HB, Bulovic V, Dresselhaus MS, Kong J. Nano Lett. 2009;9:30.

29. Lee Y, Bae S, Jang H, Jang S, Zhu SE, Sim SH, Song YI, Hong BH, Ahn JH. Nano Lett. 2010;10:490.

30. Krasheninnikov AV, Nieminen RM. Theor Chem Acc. 2011;129:625–630.

31. Hu FM, Ma TX, Lin HQ, Gubernatis JE. Phys Rev B: Condens Matter Mater. Phys. 2011;84:075414.

32. Ambrosi A, Pumera M. Nanoscale. 2014;6:472–476.

33. Wang Y, Zheng Y, X Xu, Dubuisson E, Bao Q, Lu J, Loh KP. ACS Nano. 2011;5(12):9927–9933.

34. Gao GL, Ren W, Xu H, Jin L, Wang Z. Ma T, Ma L, Zhang Z, Fu Q, Peng L, Bao X, Cheng H. Nature Commun. 2012;3:699.

35. de la Rosa CJL, Sun J, Lindvall N et al. App Phys Lett. 2013;102(2). Article ID 022101.

36. Wang XH et al. Small. 2014;10:694–698.

37. Cherian CT, Giustiniano F, Martin-Fernandez I, Andersen H, Balakrishnan J, Ozyilmaz B. Small. 2015;1:189–194.

38. Fang W, Hsu AL, Caudillo R, Song Y, Birdwell AG, Zakar E, Kalbac M, Dubey M, Palacios T, Dresselhaus MS, Araujo PT; Kong J. Nano Lett. 2013;13:1541.

39. Griep MH, Sandoz-Rosado E, Tumlin TM, Wetzel E. Nano Lett. 2016;16(3):1657–1662.

List of Symbols, Abbreviations, and Acronyms

AFM	atomic force microscopy
Ar	argon
BLG	bilayer graphene
C	carbon
CH_4	methane
Cu_2O	cuprous oxide
Cu	copper
CVD	chemical vapor deposition
DI	deionized
$FeCl_3$	iron chloride
FET	field-effect transistor
FWHM	full width at half maximum
H_2	hydrogen
HCl	hydrogen chloride
KOH	potassium hydroxide
Ni	nickel
I-V	current-voltage
O_2	oxygen
PMMA	poly(methyl methacrylate)
Si	silicon
SiO_2	silicon dioxide
SLG	single-layer graphene
TLG	trilayer graphene

1 (PDF) DEFENSE TECHNICAL INFORMATION CTR DTIC OCA

2 (PDF) DIR ARL
RDRL CIO L
IMAL HRA MAIL & RECORDS MGMT

1 (PDF) GOVT PRINTG OFC
A MALHOTRA

3 (PDF) US ARMY RSRCH OFC
RDRL ROE L
J QIU
RDRL ROE M
J PRATER
M VARANASI

1 (PDF) US ARMY ARDEC
RDAR MEF S
C PEREIRA

24 (PDF) ARL
RDRL DE
T O'REGAN
RDRL SEE
J MULCAHY
M ROY
S STRNAD
M SUNAL
RDRL SER
P AMIRTHARAJ
RDRL SER E
G BIRDWELL
F CROWNE
P SHAH
T IVANOV
M DERENGE
RDRL SER L
W NOTHWANG
M DUBEY
E ZAKAR
B NICHOLS
M CHIN
R BURKE
A MAZZONI
S NAJMAEI
B ISAACSON
C KNICK
D POTREPKA
M ERVIN
R BENOIT

INTENTIONALLY LEFT BLANK